Effect of Al-Doping on Electrochemical Performance of LiMn$_2$O$_4$

Xinghua Liang[*], Shuaibo Zeng, Yusi Liu, Tianjiao Liu, Lin Shi and Chaochao Ye

Guangxi Science and Technology University, Liuzhou 545006, P.R. China

*Corresponding author: Tel: +86 18648863918; E-mail: lxh304@aliyun.com.cn

Spinel LiMn$_2$O$_4$ and LiAl$_x$Mn$_{2-X}$O$_4$(G^X, X = 0, 1, 2, 3, 4) have been synthesized by solid-state method. The synthesized samples were characterized by following methods: X-ray diffraction, scanning electron microscopy. Results showed that LiAl$_{0.3}$Mn$_{1.7}$O$_4$(G^3) was spinel structure which space group was Fd3m. The spinous substances were not observed on its spherical-structured surface. Experimental battery E^X(X = 0, 0.1, 0.2, 0.3, 0.4) was assembled by using G^X as cathode electrode, active carbon as conductive agent and Li plate as the anode electrode. The E^X(X = 0, 0.1, 0.2, 0.3, 0.4) was characterized by electrochemical impedance spectroscopy, cyclic voltammetry and charge-discharge studies. Results indicated that Al-substitution decreased the internal resistance of E^X. Charge-discharge cycling studies and cyclic voltammetry test showed that Al-substitution substantially improved the capacity retention of the E^X.

Keywords: Lithium ion battery, XRD, SEM, Electrochemical performance.

INTRODUCTION

Spinel LiMn$_2$O$_4$ is the most broadly studied cathode material for lithium rechargeable batteries owing to advantages including easy preparation, low cost, non-toxicity, economical and environmental friendly and relatively high energy density[1-5]. The solid-state method, because of its simple processes and easily control and lower requirement in equipment, has been a common way to produce cathode material of lithium ion batteries on a large scale. However, cathode material has not been mixed evenly, which could possibly lead to lower substance purity, Mn$_2$O$_3$ being produced and breakdown of the spinel lattice. At the later stage of discharging, on the surface of Mn^{3+} easily takes place the disproportionation reaction[6-7]: $2Mn^{3+}(s) \rightarrow Mn^{4+}(s) + Mn^{2+}(l)$, while the liquid Mn^{2+} dissolves in the electrolyte. It is the reason why the capacity of spinel LiMn$_2$O$_4$ fades rapidly in charge-discharge cycle. The structure of spinel could be destroyed and impedance of the battery increases while coulomb effect dwindles under the condition of high temperature and large current charge-discharge process. Above all of these can limit the commercialization of LiMn$_2$O$_4$. In order to solve these problems, people have proposed an effective strategy[8-10] to substitute Mn^{3+}, which contributes to improve conductivity of the cathode materials as well as the electrochemical performance of the battery. Krins *et al.*[11] and Wu *et al.*[12] doping Ti^{4+} greatly improved the electrochemical property of LiMn$_2$O$_4$. Because the binding energy of Cr-O (1142 KJ/mol) is much higher

than that of Mn-O (946 KJ/mol)[13-15], doping Cr^{3+} propelled the formation of a stable three-dimensional structure and decreasing of the dissolved load of Mn^{2+}, which weakened the Jahn-Teller effect. Even though Thirunakaran *et al.*[16], Wang *et al.*[17] and Lee *et al.*[18] doping Al^{3+} by sol-gel method bettered the stability and cyclic performance of LiMn$_2$O$_4$, the discharge capacity turned out to be 105 mAhg^{-1} after 50 cycles at 0.2 C.

In this paper, we prepared the cathode material of the Al-substitution (G^X) lithium ion battery by solid-state method, which Li plate was used as anode electrode and LiPF$_6$ concentrated 1 mol L^{-1} (volume proportion of EC/DNC being1:1) used as electrolyte, Celgard2300 as diaphragm to assemble the battery (E^X). Structure and morphology of the G^X were characterized by XRD and SEM. Cyclic voltammograms and AC impedance were used to analyze the surface state change of E^X electrode after charge-discharge. A higher capacity cathode electrode after storage was given by solid-state method.

EXPERIMENTAL

Atmosphere box furnace (KBF13Q); X ray diffraction (DX-2700); scanning electron microscope (EVO18); vacuum glove box (ZKX-2); high-precise testing system for battery performance (CT3008W); electrochemical workstation (CHI600D).

Lithium acetate (99.9 % pure), manganese acetate (99.9 % pure) and Al$_2$O$_3$ (99.9 % pure) were fully mixed with a stoichiometric mole ratio of Li:Mn:Al = 1.2:(2-X):X (X = 0; 0.1; 0.2; 0.3; 0.4). Then preheated all of them in the atmosphere furnace

at 450 °C for 4 to 6 h, keeping heating rate below 10 °C min^{-1}. After furnace cooling, increased the temperature to 750 °C and heated them for 50 to 72 h, keeping heating rate below 10 °C min^{-1}. After the furnace cooling again, black G^X (X = 0, 1, 2, 3, 4) can be obtained.

Battery assembly: Cathode paste are formed by mixing G^X (active material) (80 wt. %), active carbon (conductive agent) (10 wt. %) and PVDF-HFP (binder) (10 wt. % polyvinylidene fluoride, PVDF, dissolved in N-methyl-2-pyrrolidone, NMP). The slurry was coated on aluminum foil substrates by doctor blade. Then aluminum foil was dried under the temperature of 80 °C and cut by the tablet machine. Using a piece of lithium metal as anode electrode, LiPF6 and EC/DNC whose concentration is 1 mol/L (1:1, volume ratio) as electrolyte and Celgard 2300 as diaphragm. The experimental batteries E^X (X = 0, 1, 2, 3, 4) can be assembled in the manual-operation box which was filled with argon gas.

RESULTS AND DISCUSSION

Analysis of X-ray diffraction: Crystal structure of the products were analyzed *via* X-ray diffraction with CuK$_\alpha$ radiation at a scanning speed of 0.03° s^{-1}, wavelength of 1.5406A, tube voltage of 40 kV, tube current of 30 mA. Fig. 1 shows the X-ray diffraction pattern of the G^X powders. It is found that the diffraction peaks at 2θ = 19.14°, 36.15°, 37.91°, 44.80°, 48.19°, 58.35°, 64.80° and 68.96° are corresponding to the crystal planes of (1 1 1), (3 1 1), (2 2 2), (4 0 0), (3 3 1), (5 1 1), (4 4 0) and (5 3 1). It showed that all five groups were spinel-type structure with *Fd3m* space group. Diffraction peaks of Mn$_2$O$_3$ were observed at 28.50°, 32.80° in groups of G^1 and G^2. And there were no diffraction peaks of Mn$_2$O$_3$ in groups of G^3 and G^4. Table-1 presented the lattice parameters and full width at half maximum (FWHM) values of (400) peak of the G^X powders. It has been demonstrated that the lower FWHM value of the (400) peak was relative to higher crystallinity of spinel LiMn$_2$O$_4$. From Table-1, it is obvious that the Al-substitution had a higher crystallinity than pure LiMn$_2$O$_4$. The G^X were relative to higher specific surface area than pure LiMn$_2$O$_4$, because of smaller lattice volume.
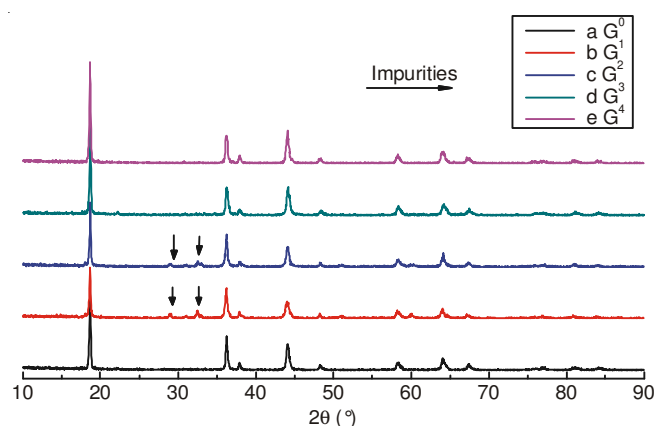
Fig. 1. X-ray diffraction pattern of the G^X powders. (a) G^0; (b) G^1; (c) G^2; (d) G^3; (e) G^4

Scanning electron microscopy: SEM test was conducted with a microscope magnification of 10000X at a voltage of 20 kV. Its studies reflected the textural and morphological

TABLE-1
LATTICE PARAMETERS OF THE SAMPLES G^X AND FWHM OF (400) PEAK

Sample	Lattice constant (a) (Å)	Lattice volume (Å^3)	FWHM of (400) peak (°)
G^0	8.242	559.8	0.1596
G^1	8.235	558.4	0.1585
G^2	8.231	557.6	0.1578
G^3	8.228	557.0	0.1576
G^4	8.217	554.8	0.1571

characteristics of the G^X. Results suggested that G^X samples had spherical structure with an average diameter size between 50 nm to 500 nm and spinous processes were not observed in Fig. 2. It means that the diaphragm could not be pierced. The structure might avoid short circuit.
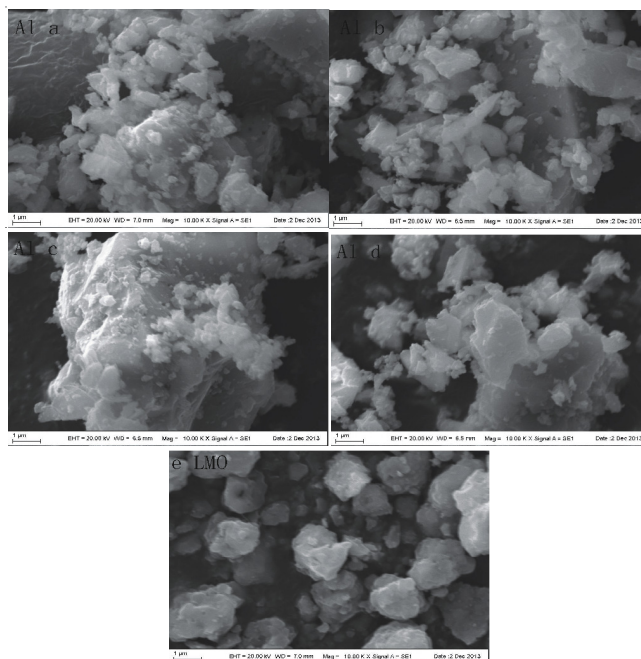
Fig. 2. SEM image of G^X powders. (a) G^1; (b) G^2; (c) G^3; (d) G^4; (e) G^0

Electrochemical impedance spectroscopy analysis: Electrochemical impedance spectroscopy was studied with a frequency range of 10 MHz to 100 KHz and amplitude of 5 mV. Fig. 3 was the spectroscope of E^X in its first process of charge-discharge. It was found that E^3 had increased Coulomb effect in the battery because of decreasing internal resistance. Doping Al^{3+} restricted the growth of electrochemical reaction impedance in large current charging-discharging; it greatly enhanced the high current charge-discharge property of the battery.

Cyclic voltammetry: Cyclic voltammetry curve was studied at electrochemical workstation with an initial potential of 3 V and a maximum of 4.4 V. Scanning rate was 0.1 mVS^{-1} with a sensitivity of $1 \times e^{-0.04}$. Test temperature was 20 °C. Fig. 4 showed the cyclic voltammetry curves of E^X (X = 0, 1, 2, 3, 4). It indicated two redox peaks of E^X: 3.97 V/3.81 V(E^0); 3.96 V/3.81 V(E^1); 4.00 V/3.85 V(E^2); 3.98 V/3.81 V(E^3); 4.00 V/3.84 6 V(E^4), which responded to the pair of charge-discharge platforms. Current of E^3 at two redox peaks were 6 and 5 mA. The reversible capacity of E^3 was also the largest area which was surrounded by two curves. It can also be certified by the charge-discharge curves.
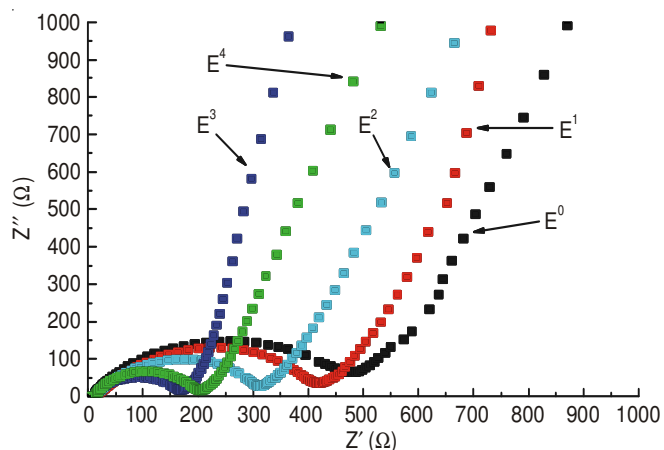
Fig. 3. Electrochemical impedance spectroscopy plots of E^X in initial charge process (E^X, X = 0, 1, 2, 3, 4)
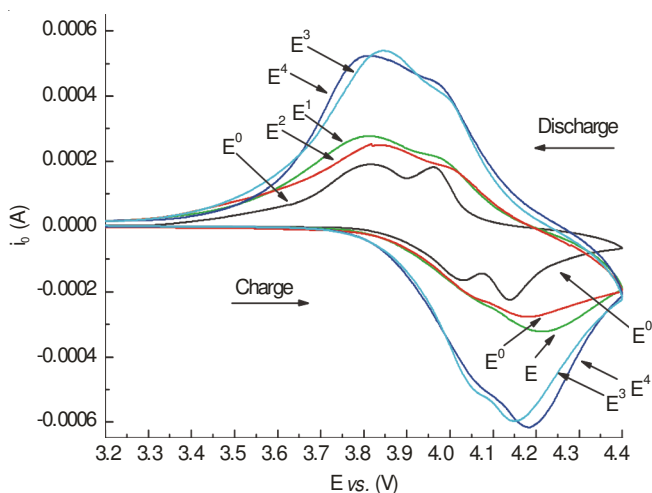
Fig. 4. First cyclic voltammograms of E^X. (E^X, X = 0, 1, 2, 3, 4)

Fig. 5. Charge-discharge curves of E^X (X = 0, 1, 2, 3, 4) at 0.1 C in the voltage range of 3.00-4.35 V *vs.* Li/Li⁺
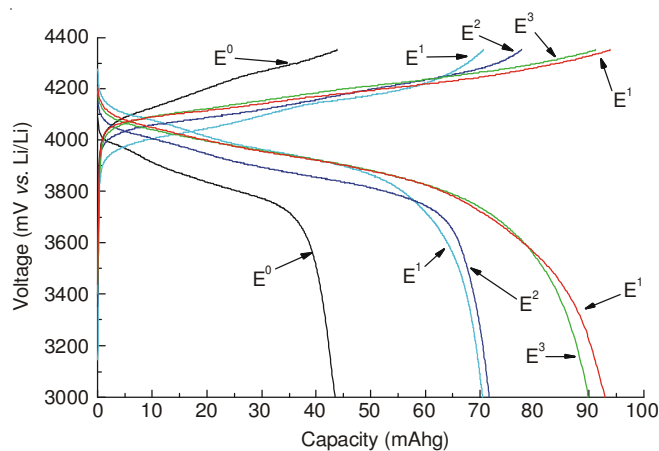
Fig. 6. Charge-discharge curves of E^X (X = 0, 1, 2, 3, 4) at 0.5 C in the voltage range of 3.00-4.35 V *vs.* Li/Li⁺
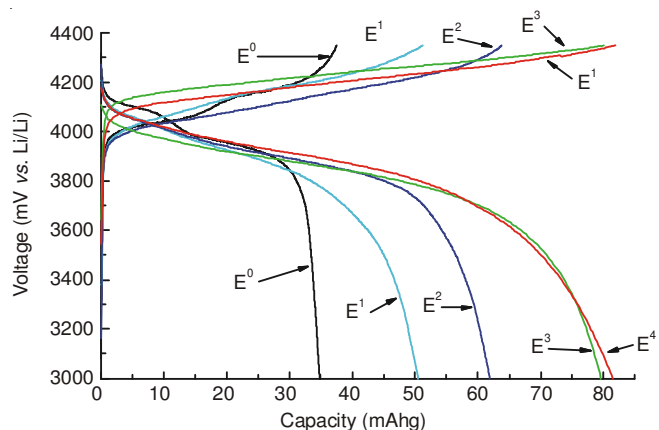
Fig. 7. Charge-discharge curves of E^X (X = 0, 1, 2, 3, 4) at 1 C in the voltage range of 3.00-4.35 V *vs.* Li/Li⁺

Analysis of charge-discharge and charge-discharge cycling studies: The charge-discharge test was carried out by Neware battery testing instrument. Current ranges output from -5 mA to +5 mA. Both measuring accuracy of current and voltage maintain at ± (0.05 % + 0.1 %). Tests were carried room temperature. Figs. 5-7 reflected the results under the initial charge-discharge current at 0.1, 0.5 and 1 C. It can be found that specific discharge capacity of cathode materials slowly went down in low current charging-discharging after Al³⁺ dopped, however, with the current increasing from 0.1 to 1 C, the discharge capacity of pure LiMn₂O₄ faded faster. Specific discharge capacity of pure LiMn₂O₄ was 35 mAhg⁻¹ at 1 C, but E^3 and E^4 were 80 and 82 mAhg⁻¹ at 1 C. Figs. 8 and 9 presented cyclic voltammetry curves after 52 cycles at 0.5 C, 1 C. It was indicated that capacities of LiMn₂O₄ without doping Al³⁺ faded obviously at 0.5 C, 1 C. In contrast, capacities of LiMn₂O₄ with doping Al³⁺ didn't fade obviously at the same condition. As a result, doping Al³⁺ can contribute to improve cyclic performance of battery; specific capacities of E^3 became 115 mAhg⁻¹, 90 mAhg⁻¹ at 0.5 C, 1 C after 52 cycles.

Conclusion

In the process of synthesizing cathode material G^X (X = 0, 1, 2, 3, 4) by solid-state method, doping Al³⁺ had influence on appearance and electrochemical performance of LiMn₂O₄.

The synthesized product remained spinel-type. Doping a small quantity of Al³⁺ caused peaks of Mn₂O₃; spinous substances were not observed on its spherical-structured surface. In addition, there was great improvement in E^X in its cyclic performance and large current charge-discharge performance. Results of cyclic voltammetry curves suggested that Al³⁺ substituted part of Mn³⁺ restricted the disproportionation reaction at later stage of discharging. Because of increased the current of redox peaks.
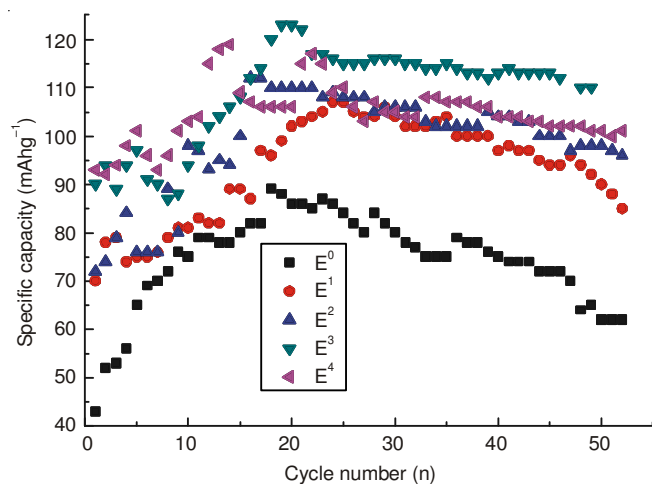
Fig. 8.   Cyclic performance of E^X (X = 0, 1, 2, 3, 4) with varying Al^{3+} doping at 0.5 C
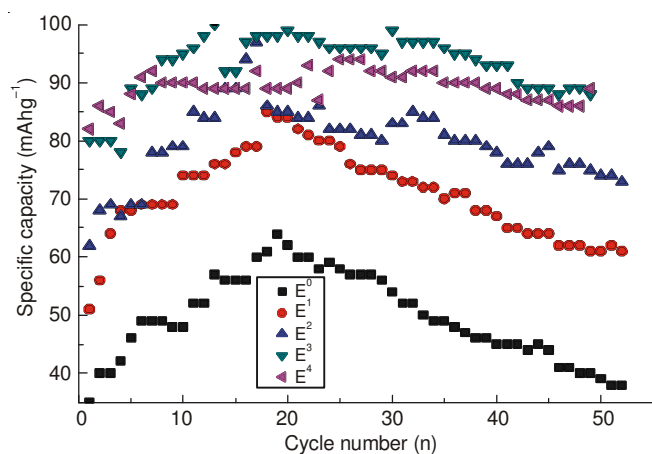
Fig. 9. Cyclic performance of E^X (X = 0, 1, 2, 3, 4) with varying Al^{3+} doping at 1 C

At rate of 0.5 C, 1 C, initial charge and discharge capacities of E^3 were 89 and 80 mAhg^{-1}, respectively which turned to be 115 and 90 mAhg^{-1} after 52 cycles.

REFERENCES

1.   H.-J. Hong, I.-S. Park, T. Ryu, J. Ryu, B.-G. Kim and K.-S. Chung, *Chem. Eng. J.*, **234**, 16 (2013).
2.   C. Chae, H. Park, D. Kim, J. Kim, E.-S. Oh and J.K. Lee, *J. Power Sources*, **244**, 214 (2013).
3.   J.-W. Lee, J.-I. Kim and K.C. Roh, *Solid State Sci.*, **14**, 1251 (2012).
4.   M.M. Joglekar and N. Ramakrishnan, *J. Power Sources*, **230**, 143 (2013).
5.   J.L. Wang, Z.H. Li, J. Yang, J.J. Tang, J.J. Yu, W.B. Nie, G.T. Lei and Q.Z. Xiao, *Electrochim. Acta*, **75**, 115 (2012).
6.   S.T. Myung, S. Komaba, N. Hirosaki and N. Kumagai, *Electrochem. Commun.*, **4**, 397 (2002).
7.   S. Komaba, N. Kumagai, T. Sasaki and Y. Miki, *Electrochemistry*, **69**, 784 (2001).
8.   H. Sahan, H. Goktepe, S. Patat and A. Ulgen, *Solid State Ion.*, **181**, 1437 (2010).
9.   H. Sahan, H. Goktepe and S. Patat, *J. Mater. Sci. Technol.*, **27**, 415 (2011).
10. D. Arumugam and G.P. Kalaignan, *Electrochim. Acta*, **55**, 8709 (2010).
11. N. Krins, F. Hatert, K. Traina, L. Dusoulier, I. Molenberg, J.F. Fagnard, Ph. Vanderbemden, A. Rulmont, R. Cloots and B. Vertruyen, *Solid State Ion.*, **177**, 1033 (2006).
12. Q.-H. Wu, J.-M. Xu, Q.-C. Zhuang and S.-G. Sun, *Solid State Ion.*, **177**, 1483 (2006).
13. C. Wu, F. Wu, L. Chen and X. Huang, *Solid State Ion.*, **152-153**, 335 (2002).
14. G.X. Wang, D.H. Bradhurst, H.K. Liu and S.X. Dou, *Solid State Ion.*, **120**, 95 (1999).
15. R. Thirunakaran, A. Sivashanmugam, S. Gopukumar, C.W. Dunnill and D.H. Gregory, *Mater. Res. Bull.*, **43**, 2119 (2008).
16. R. Thirunakaran, A. Sivashanmugam, S. Gopukumar, C.W. Dunnill and D.H. Gregory, *J. Phys. Chem. Solids*, **69**, 2082 (2008).
17. J.L. Wang, Z.H. Li, J. Yang, J.J. Tang, J.J. Yu, W.B. Nie, G.T. Lei and Q.Z. Xiao, *Electrochim. Acta*, **75**, 115 (2012).
18. J.-F. Lee, Y.-W. Tsai, R. Santhanam, B.J. Hwang, M.-H. Yang and D.-G. Liu, *J. Power Sources*, **119-121**, 721 (2003).